

pubs.acs.org/cm Article

Investigation of Thermally Activated Delayed Fluorescence in Donor-Acceptor Organic Emitters with Time-Resolved Absorption Spectroscopy

Lloyd Fisher, Jr., Ricardo Javier Vázquez, Madeleine Howell, Angelar K. Muthike, Meghan E. Orr, Hanjie Jiang, Betsy Dodgen, Dong Ryun Lee, Jun Yeob Lee, Paul Zimmerman, and Theodore Goodson, III*



Cite This: Chem. Mater. 2022, 34, 2161–2175



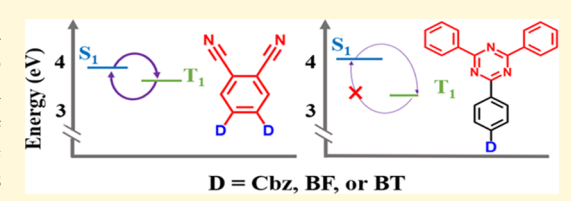
ACCESS

Metrics & More

Article Recommendations

Supporting Information

ABSTRACT: In this contribution, we utilize multiple time-resolved and nonlinear optical measurements and quantum chemical simulations to investigate the excited-state dynamics of organic chromophores with thermally activated delayed fluorescent (TADF) characteristics. We are most interested in probing the influence of a phenylene linker on the photophysical properties of emitters composed of carbazole-based donors linked to either a phthalonitrile (PN) or diphenyltriazine (Trz) acceptor. The



PN-acceptor compounds display a near double-fluorescence quantum yield (Φ_F) enhancement in oxygen-free conditions. The fluorescent lifetime measurements indicate that the Trz-acceptor compounds are more efficient fluorescence emitters and quickly go from a delocalized to localized state. They also reveal that only the PN-acceptor compounds display a long-lived emissive lifetime component associated with TADF activity. Analysis of the nanosecond transient absorption spectra and kinetics reveals long-lived excited-state absorption (ESA) bands associated with triplet states for the PN-acceptor compounds. No ESA bands were observed for the Trz-acceptor compounds, despite observing a quantum yield enhancement for the Trz-acceptor compounds after oxygen purging. From the transient absorption measurements, it was determined that the PN-acceptor compounds have reverse intersystem crossing rates (k_{rISC}) that are able to compete with other triplet decay pathways. From quantum chemical calculations, it is proposed that inclusion of the phenylene linker prevents sufficient highest occupied molecular orbital/lowest unoccupied molecular orbital separation and suppresses TADF activity and that directly linking multiple donors to the acceptor will aid in achieving TADF activity.

1. INTRODUCTION

Thermally activated delayed fluorescence (TADF) is an emissive mechanism proposed for use in organic light-emitting diodes (OLEDs) to achieve internal quantum efficiencies ($\eta_{\rm IQE}$) of ~100%. The high $\eta_{\rm IQE}$ is ascribed to the use of all charge carriers through the conversion of nonemissive triplets into emissive singlets via a thermally-assisted reverse intersystem crossing (rISC) mechanism. This mechanism is reportedly made possible by a small energy gap (<0.1 eV) and sufficient spin—orbit coupling (SOC) between the singlet—triplet manifolds. As a result, purely organic TADF materials have attracted immense attention as potential replacements for rare metal-containing phosphorescent emitters in blue light-emitting diodes due to their advantageous properties such as optical tuning via synthesis, device flexibility, and relatively lower costs. 3,9,10

The different decay pathways of excited states, including the TADF process, are displayed in Figure 1 along with their relative rates. $^{11-13}$ Upon photoexcitation, the singlet-excited state (S_1) is populated. This state can undergo fluorescence, which will return it to the ground state (S_0) , or undergo

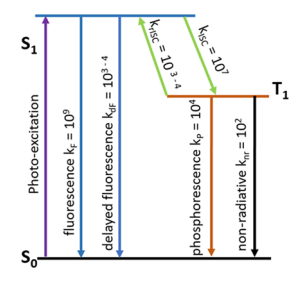


Figure 1. Decay processes of excited states and associated rate constants. $^{11-13}$

intersystem crossing (ISC), which will populate the triplet excited state (T_1) . For T_1 to be populated, the rate of ISC

Received: October 26, 2021 Revised: February 9, 2022 Published: February 22, 2022





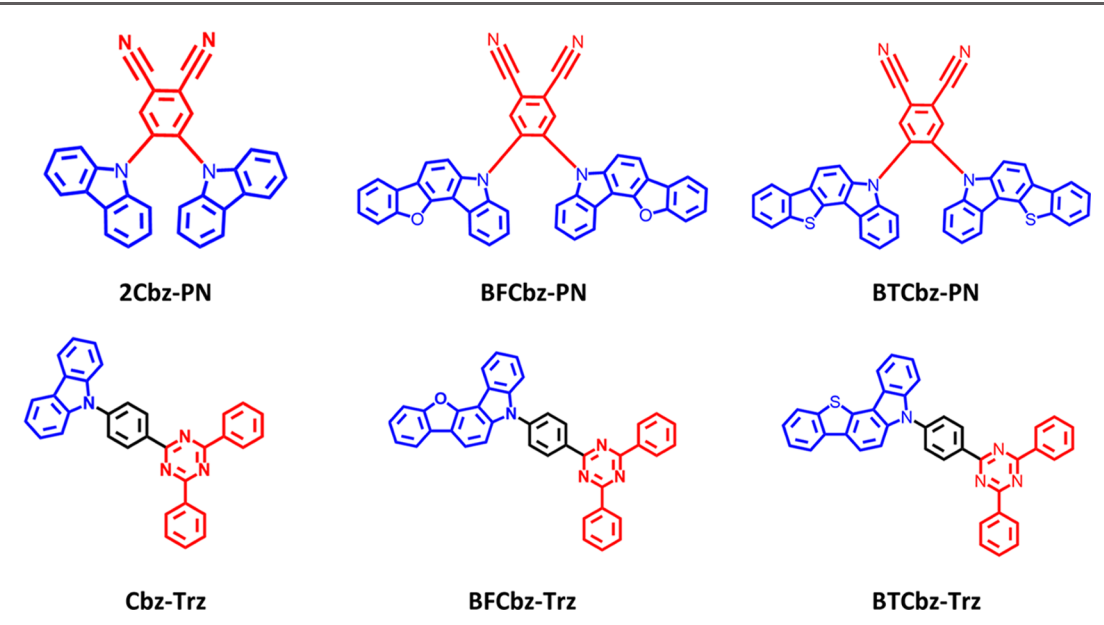


Figure 2. Structures of investigated chromophores (PN series above and Trz series below), where the donor unit is blue and the acceptor unit is red.

 $(k_{\rm ISC})$ must be able to compete with the rate of fluorescence $(k_{\rm F})$. Once populated, the T $_1$ state can undergo phosphorescence, nonradiative decay, or rISC. The TADF mechanism depends on the rate of rISC $(k_{\rm rISC})$ out-competing the rates of phosphorescence $(k_{\rm P})$ and nonradiative decay of T $_1$ $(k_{\rm nr})$. Previous investigations into $k_{\rm rISC}$ have determined that efficient TADF depends on $k_{\rm rISC} > 10^3.^{1,11,14}$ It is apparent that TADF is an unusual process that requires contributions from many different components, including a small singlet—triplet energy gap $(\Delta E_{\rm ST})$ and strong SOC. 7,11

The design principle of achieving a small singlet-triplet energy gap (ΔE_{ST}) in fully organic chromophores consists of synthesizing a donor-acceptor complex with a partial break in the conjugation between the donor-acceptor junction. 1,7,15-18 This partial break allows for minimal overlap between the highest occupied molecular orbital (HOMO) and the lowest unoccupied molecular orbital (LUMO). By maximizing the dihedral angle of the junction, one can minimize ΔE_{ST} and enhance k_{rISC} . Recent publications indicate that parameters other than HOMO/LUMO separation play an important role in the TADF process. 1,3,14 One such report highlights that maximizing spatial separation between the HOMO and LUMO does not necessarily result in effective energy transfer between the singlet and triplet manifolds. Instead, it suggests that enhancing the charge transfer (CT) character of the triplet state and increasing SOC between S_1 and T_1 may be a more effective route to enhancing $k_{\rm rISC}$. Yet, another report suggests an alternative method of achieving TADF by utilizing multiple resonance states instead of the traditional donoracceptor design. 19 Unfortunately, the critical spectroscopic measurements needed to fully comprehend the rISC mechanism are not conducted on the majority of newly synthesized materials designed for TADF applications. The field has traditionally relied on steady-state and time-resolved microsecond measurements to determine TADF activity. However, some investigations have been conducted utilizing time-resolved spectroscopic techniques.

Choi et al.²⁰ reported on the impact of solvent polarity and local environment on the excited-state dynamics of a TADF

emitter via femtosecond transient measurements. They observed that the excited-state dynamics of DPA-AQ-DPA were completed within tens of picoseconds in a polar solvent, indicating that ISC did not occur. However, in a nonpolar solvent, the excited-state dynamics continue past 3 ns, indicating that a triplet excited state had formed. As ISC to the triplet state is an important step for the TADF process, it was determined that for this compound, the TADF mechanism does not occur in high polarity solvents. This is due to the interactions between the intramolecular charge transfer (ICT) state and polar solvents causing stabilization of this state. If the energy of the ICT state is made to be less than that of the $^{3}\pi\pi^{*}$, due to the interactions of ICT and polar solvent, then ISC from the singlet to triplet manifolds and, subsequently, TADF is inhibited. They found that in a low polarity solvent, the ICT state is at a higher energy than the ${}^3\pi\pi^*$, allowing for ISC to the triplet state to occur. This finding shows the importance of considering which solvent is used for spectroscopic measurements in determining TADF activity.

He et al.²¹ performed nanosecond transient absorption spectroscopy (nsTAS) measurements on donor-acceptor complexes. While the compounds in their report were not determined to be TADF active, their findings provide a good demonstration of the merits of this spectroscopic technique for determining a compound's excited-state dynamics. They found broad excited-state absorption (ESA) bands that were in the same region as the fluorescence emission. However, due to the long time delay of the measurement, the fluorescence signal had little contribution to the transient spectra. The excited states observed via nsTAS displayed long lifetimes which were enhanced in purged solutions, indicating that the excited states are triplets. They found that the ICT state is stabilized in polar solvents, while the triplet state is largely unaffected. Their results also support that compounds with a significant degree of CT character display smaller quantum yields in polar solvents due to strong interactions between the large dipole moments of the ICT state and the solvent.

Franca et al.²² utilized nsTAS, in combination with other techniques, to reveal the importance of the triplet local exciton

(3LE_{A n\u03c0\u03c0\u03c0)} state in TADF. Through the transient absorption measurements, they observed the population of the ${}^{3}\text{LE}_{\pi\pi^{*}}$ from the ¹LE_A. They report a TADF pathway for ACRSA, where the ${}^{3}LE_{A n\pi^{*}}$ state couples to the triplet charge-transfer (3CT) and singlet charge-transfer (1CT) states, allowing for rISC. The energy of the ${}^3LE_{A\;n\pi^*}$ state is increased with increasing solvent polarity, while the energies of the ³CT and ¹CT are decreased. This increases the energy gap between these states and impedes the rISC mechanism. Also utilizing nsTAS, Vázquez et al. determined that the emitter BCC-TPTA lacked a long-lived emissive component and ESA bands characteristic of triplet states.³ Conducted in solution, the nsTAS measurements revealed that BCC-TPTA had excitedstate dynamics similar to a fluorescent compound with minimal long-lived triplet-excited states. This was despite BCC-TPTA displaying a quantum yield enhancement after purging oxygen from solution. A method for approximating k_{rISC} was also developed using the nsTAS technique to directly observe triplet-state dynamics free of guest-host interactions. These reports demonstrate the capabilities of the nsTAS technique for probing the photophysics of various compounds and determining their emissive mechanism.

In this contribution, we utilize multiple steady-state and time-resolved spectroscopic techniques, with an emphasis on nsTAS, to investigate the TADF activity of emitters with carbazole and carbazole-derivatives as donors and phthalonitrile (PN) or triazine (Trz) as acceptors (Figure 2). We focus on determining the influence of molecular structure, specifically the influence of a linker between the donor and the acceptor, on TADF activity. Our results reveal a relationship between the differences in donor strength and the rate of rISC (k_{rISC}). It is widely accepted that enhancement of the fluorescence quantum yield is evidence that the excitedstate decay dynamics of an emitter is governed by a delayed fluorescence mechanism. However, our measurements reveal that this Φ_F enhancement is not the only metric of importance. The nsTAS technique reveals a connection between observable triplet transient states and the rISC mechanism and allows us to determine a relationship between donor strength and k_{rISC} intensity. We also propose a connection between the choice of host material and the change of the emitter's photophysics.

2. EXPERIMENTAL SECTION

2.1. Synthesis and Characterization. The reaction procedures of 5-(4-(4,6-diphenyl-1,3,5-triazin-2-yl)phenyl-5*H*-benzofuro[3,2-c]-carbazole (BFCbz-Trz), 4,5-bis(benzofuro[3,2-c]-carbazol-5-yl)phthalonitrile (BFCbz-PN), and 4,5-bis(benzo[4,5]thieno[3,2-c]-carbazol-5-yl)phthalonitrile (BTCbz-PN) have been previously described. 23,24 What follows is the reaction procedure for 5-(4-(4,6-diphenyl-1,3,5-triazin-2-yl)phenyl)-5*H*-benzo[4,5]thieno[3,2-c]-carbazole (BTCbz-Trz). Sodium hydride, 2-chloro-4,6-diphenyl-1,3,5-triazine, and (4-fluorophenyl)boronic acid (TCI Chem. Co.) were used without further purification. Tetrahydrofuran (THF) was distilled over sodium and calcium hydride.

Here, sodium hydride (0.07 g, 3.06 mmol) was then washed with hexane three times and dried under vacuum. SH-Benzo[4,5]thieno-[3,2-c]carbazole (0.46 g, 1.68 mmol) was dissolved in THF (50 mL) and added to the flask. The reaction mixture was stirred for 30 min at room temperature under inert N_2 atmosphere, and then 2-(4-fluorophenyl)-4,6-diphenyl-1,3,5-triazine (0.50 g, 1.53 mmol) was added. The reaction was quenched with distilled water (10 mL) at the 12 h mark. The reaction mixture was extracted with MC and distilled water three times. The organic layer was dried over MgSO₄ and purified by column chromatography on silica gel using hexane/dichloromethane (1:2) as the eluent. The product was purified by

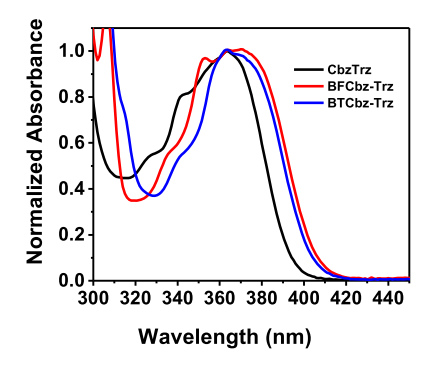
thermal gradient sublimation and pure BTCbz-Trz was obtained as a pale-yellow powder.

- **2.2. Steady-State Absorption and Emission.** The absorption and emission measurements were carried out in dilute toluene solutions. The absorption spectra were collected via an Agilent 8341 spectrophotometer. The emission spectra were collected using a FluoroMax-4 fluorimeter, with entrance and exit slits set to 1.0 nm and an integration time of 1.0 s. Quartz cuvettes with 1.0 cm path lengths were used for all steady-state measurements.
- **2.3. Fluorescence Quantum Yield Calculation.** The fluorescence quantum yields (Φ_F) were calculated utilizing the Williams comparative method. ^{25,26} A series of solutions of decreasing concentration were utilized for the calculations. The optical densities of the solutions used for these measurements started at 0.10 and were systematically halved. The quantum yields were calculated using eq 1

$$\Phi_{\rm F} = \Phi_{\rm STD} \frac{{\rm Grad}_{\rm x} \eta_{\rm x}^2}{{\rm Grad}_{\rm STD} \eta_{\rm STD}^2} \tag{1}$$

where $\Phi_{\rm F}$ is the calculated quantum yield, η is the refractive index of the solvent, and Grad is the slope obtained from plotting the fluorescence area versus the optical density. The subscripts STD and x refer to the standard and investigated compounds, respectively. The quantum yields for the investigated chromophores were calculated using Coumarin 6 in ethanol and Cascade Blue in water as standards. 27,28 Oxygen-free $\Phi_{\rm F}$ was obtained by purging the solutions via nitrogen bubbling for 10 min. The emission spectra were collected on a Cary Eclipse fluorescence spectrometer with slits set at 1.5 nm. Quartz cuvettes with 1.0 cm path lengths were used for all measurements.

- **2.4. Two-Photon Absorption.** The two-photon absorption (TPA) spectroscopy technique, which has been previously described, was used to investigate the CT properties of the investigated chromophores in solution. ^{25,29-34} The optical densities of the solutions were kept to 0.10. TPA was conducted utilizing a modelocked Ti:Sapphire laser tunable from 700 to 900 nm, delivering 110 fs output pulses at a repetition rate of 80 MHz. Emission scans were conducted at 800 nm excitation while scanning 400-700 nm emission. The emission detection wavelength for the power dependence scan was determined by the emission wavelength that produced the highest number of counts at 400 nm excitation (by simultaneously absorbing two 800 nm photons). Rhodamine B was used as the standard. Input power from the laser was adjusted via a variable neutral density filter. Two-photon power-dependent fluorescence intensity was utilized to determine the TPA cross section using the two-photon emission fluorescence method, in which a loglog plot of counts per second of two-photon induced emission versus beam power (mW) was constructed for each sample.
- 2.5. Time-Resolved Fluorescence Up-Conversion. Time resolved fluorescence decay measurements of the chromophores were detected at an up-converted wavelength of 287 nm using a FOG-100 (CDP Instruments, Inc.) system, a technique described previously.^{35–38} A mode-locked Ti:Sapphire (Tsunami, Spectra Physics) laser source of 790 nm was used. The source beam underwent frequency doubling by passing through a β -barium borate (BBO) nonlinear crystal. By second harmonic generation, 395 nm light was produced which acted as the excitation source for the sample in solution phase (1 mm thick rotating sample cell). The remaining 790 nm light (the gate) passed through an optical delay line, which induced a delay in time by adjusting the path length of the gate beam. Both the gate and the sample fluorescence passed through a BBO crystal. Sum frequency generation occurred when the gate pulse entered the BBO crystal at the same time as the sample fluorescence. As delay is introduced to the gate beam, fluorescence decay can be detected. The detected (up-converted) light is collected by a monochromator and a photomultiplier tube (R1527P, Hamamatsu).
- **2.6. Time-Correlated Single Photon Counting.** The time-correlated single photon counting (TCSPC) technique, which has been previously described, was used to investigate the components of fluorescence and the fluorescence decay lifetime of the investigated



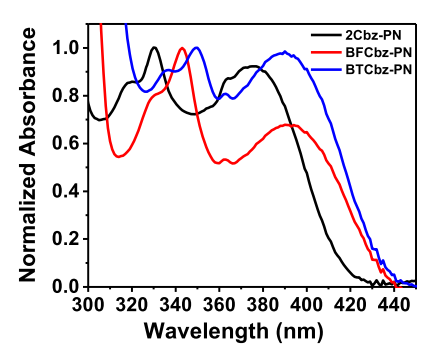


Figure 3. Absorbance spectra of Trz-acceptor (left) and PN-acceptor compounds (right) in toluene.

Table 1. Photophysical Properties of Investigated Chromophores in Toluene

compound	abs max (nm)	extinction coefficient $(M^{-1} cm^{-1})$	emission max (nm)	$\Phi_{\text{unpurged}}/\Phi_{\text{purged}}$ (%)	TPA cross section (GM)
Cbz-Trz	363	2.37×10^4	420	97/100	1.01
BFCbz-Trz	370	1.16×10^{5}	432	91/100	14.9
BTCbz-Trz	370	9.97×10^{3}	432	98/100	8.8
2Cbz-PN	380	1.36×10^{5}	473	17/21	15.9
BFCbz-PN	395	2.34×10^{5}	500	15/28	44.4
BTCbz-PN	395	1.79×10^{5}	500	12/24	21.8

chromophores. 3,14,25,32,33 The decay lifetimes were determined by fitting log plots of the obtained spectra to a linear fit. The measurements were conducted in dilute solutions in oxygen-rich (unpurged/air) and oxygen-free (purged) environments. The solutions were purged by bubbling nitrogen for 10 min. The laser used for the TCSPC measurements was a Kapteyn Murnane (KM) mode-locked Ti-sapphire laser. The output beam of the KM laser was at a wavelength of 800 nm and a pulse duration of \sim 30 fs. The output beam was frequency-doubled using a nonlinear BBO crystal to obtain a 400 nm beam. The beam was focused on the sample cuvette (1.0 cm path length) using a lens with a focal length of 11.5 cm. The emission collection was done perpendicular to the incident beam with the help of a monochromator, while the output of the monochromator was coupled to a photomultiplier tube. The monochromator was set to detect each samples' respective fluorescence maximum.

2.7. Nanosecond Transient Absorption Spectroscopy. The absorption and decay lifetime of emissive and nonemissive transient states were investigated using nsTAS, which has been previously described.^{3,14,32} A LP980 (Edinburgh) transient system, that contains a photomultiplier tube, was coupled with a Spectra-Physics QuantaRay Nd:YAG nanosecond pulsed laser and a GWU optical parametric oscillator tunable from 206 to 2600 nm for the pump beam. For this report, the pump beam was set to each sample's respective absorbance maximum. A pulsed broadband xenon lamp beam was used to probe the excited states. These measurements were conducted in both oxygen-rich and oxygen-free solutions.

2.8. rISC Calculations. The purged ESA lifetimes, obtained from nsTAS, were used to calculate the rISC rate ($k_{\rm rISC}$) using eq 2^{14}

$$k_{\text{rISC}} = k_{\text{triplet}} * \Phi_{\text{TADF}}$$
 (2)

where k_{triplet} is the rate of triplet state decay and Φ_{TADF} is the direct difference between the purged and unpurged Φ_{F} . This method allows for the determination of k_{rISC} free of guest—host interactions and by directly observing triplet-state decay.

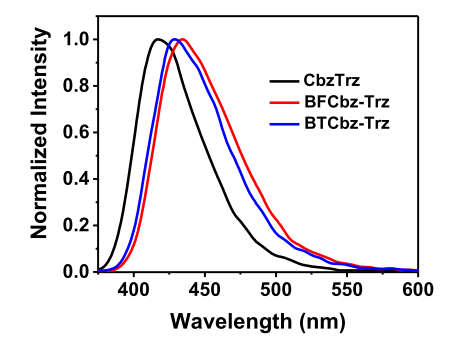
2.9. Quantum Chemical Calculations. Quantum chemical simulations were performed on all Trz- and PN-acceptor chromophores to gain insight on how the molecular structure affects the excited-state dynamics and TADF activity. Atomistic models of the Trz- and PN-acceptor chromophores were constructed with no truncation of the chromophore structure. Ground-state (S_0) geometry optimizations were performed using density functional theory (DFT), and excited singlet (S_1) and triplet (T_1) state geometries were optimized using time-dependent DFT (TD-DFT). Optimizations

were performed with B3LYP (hybrid) and ωB97X-D (rangeseparated hybrid^{39,40}) with 6-31G* as the basis set. Single-point energies were performed to determine the energies of excited singlet and triplet states for all optimized geometries using TD-DFT with functionals B3LYP and ω B97X-D and basis set 6-31G* in the gas phase. These computations provided the singlet-triplet energy gaps $(\Delta E_{\rm ST})$. SOC constants $(V_{\rm SOC})$ were calculated to determine the coupling between the S_1 and T_1 from the optimized excited triplet state geometries using TD-DFT with functionals B3LYP and ω B97X-D and basis set 6-31G* in the gas phase. Using $\Delta E_{\rm ST}$, $V_{\rm SOC}$, and single-point computations, the rISC rates for all Trz- and PN-acceptor chromophores were calculated. The formulas used for rISC rate calculations, which have been previously described, are provided in the Supporting Information. ^{1,41,42} Natural transition orbitals (NTOs) from TD-DFT were visualized using IQMOL with an isovalue of 0.07 Å⁻³. All quantum chemical computations were performed using Q-Chem 5.2 software package.45

3. RESULTS

3.1. Steady-State Absorption Measurements. The absorbance spectra of the investigated chromophores are displayed in Figure 3. Cbz-Trz has a broad absorbance band with a maximum absorbance at 360 nm, which can be attributed to ICT between the carbazole donor and the Trzacceptor. 44,45 Various shoulders can also be observed in the absorbance spectrum which are assumed to be the result of intramolecular $\pi - \pi^*$ transitions. Interestingly, the peak and shoulders are red-shifted when either benzofurocarbazole (BF) or benzothienocarbazole (BT) is used as the donor unit. This shift indicates that these transitions are stabilized due to both BF and BT being stronger donors than carbazole.²¹ Slight broadening in the absorbance range is also observed with the replacement of carbazole with BF or BT. This broadening has been attributed to increased donor contribution, oscillator strength, and steric hindrance in previous studies on carbazole derivatives.44-4

The steady-state absorbance spectrum of 2Cbz-PN displays two prominent absorption peaks at 330 and 370 nm for the first and second peaks, respectively. These dual bands are characteristic of donor—acceptor compounds with CT character. 46,48,49 Various shoulders are also observed, assumed



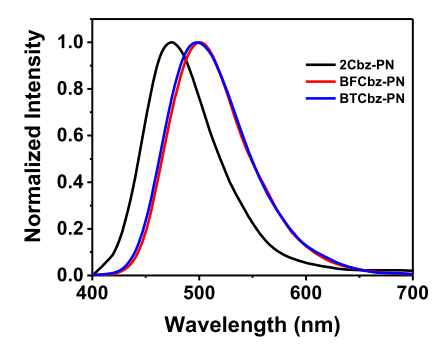
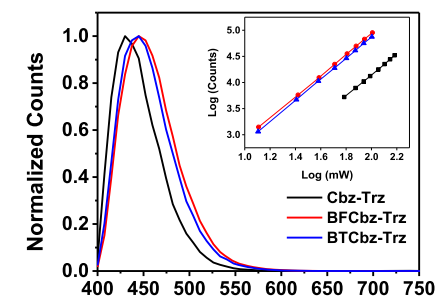


Figure 4. Fluorescence spectra of Trz-acceptor (left) and PN-acceptor compounds (right) in toluene.



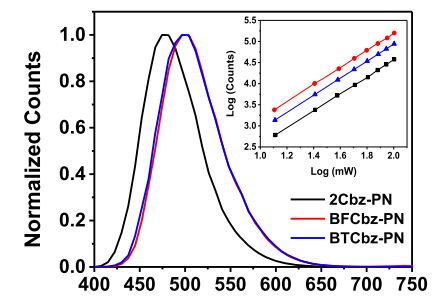


Figure 5. Two-photon induced fluorescence scans of the Trz-acceptor (left) and PN-acceptor (right) compounds in toluene. Insets are logarithmic plots of TPA power dependence versus fluorescent intensities.

to be the result of different transitions. The high energy band has been attributed to the π - π * transition, while the second lower energy band has been attributed to the $n-\pi^*$ transition. 20,24 Similar to the Trz-acceptor compounds, a red shift is observed when the carbazole unit is replaced with BF or BT. Such shifts in absorbance bands have been observed for similar carbazole derivatives.^{2,49} The red shift is attributed to the BF and BT substituents providing greater donor contribution and increasing π -conjugation. Comparison between the absorption spectra of the two series reveals that the PN-acceptor compounds have a slightly broader absorption spectrum than the Trz-acceptor compounds. The extinction coefficients provide some information on the photoabsorption capabilities of the compounds (Table 1). It is clear from the calculations that almost each PN-acceptor compound is more efficient at absorbing light than their Trz-counterpart by nearly an order of magnitude or greater. BFCbz-Trz is an exception to this as it has an extinction coefficient of 1.16×10^5 only slightly less than BFCbz-PN.

3.2. Fluorescence Measurements. The fluorescence emission spectra of all compounds are displayed in Figure 4. Cbz-Trz displays a broad emission with a maximum at 420 nm. A slight red shift in emission maximum is observable when the carbazole donor is replaced with BF or BT along with a slight broadening of the emission range. These emissions have been attributed to relaxation of the ICT state. The red shift is likely due to the stronger donors stabilizing the ICT state and increasing the dihedral angle between the donor and the phenylene linker. He is the following the stronger donors are the donor and the phenylene linker.

2Cbz-PN also displays a broad emission with a single peak at 473 nm, suggesting emission from a singlet excited state. A slight red shift in the emission spectra is observed when BF or BT is the donor group. This red shift is likely the result of the ICT state being stabilized by the stronger donor groups.^{2,10,44,47} The red shift could also be influenced by the electron-donating ability of BF or BT. As 2Cbz-PN has the

weaker donor unit, its emission is at a shorter wavelength. It is interesting that the degree of red shift is greater for the PN-acceptor compounds than the Trz-acceptor compounds, being \sim 27 and \sim 12 nm, respectively. This difference is likely due to there being two donor groups for the PN-acceptor compounds, causing greater distortion between the donors. It is also possible that having two donor groups increases π -conjugation, which has been observed to tune the emission wavelength. 47,48

The fluorescence quantum yield ($\Phi_{\rm F}$) values, which were calculated before and after the oxygen-purging process, are displayed in Table 1. Cbz-Trz has an unpurged $\Phi_{\rm F}$ of 97%, indicating that it has a great deal of π -conjugation and CT character. The $\Phi_{\rm F}$ values of BFCbz-Trz and BTCbz-Trz were equally impressive at 91 and 98%, respectively. Each compound displayed a $\Phi_{\rm F}$ enhancement to 100% with oxygen purging. Such a large $\Phi_{\rm F}$ suggests that these compounds are highly efficient fluorescent compounds. Thus, the observed enhancement could be the result of oxygen no longer quenching singlet states. S2

The PN-acceptor compounds display much smaller $\Phi_{\rm F}$ values. Unpurged $\Phi_{\rm F}$ of 2Cbz-PN was calculated to be 17%, with the values for BFCbz-PN and BTCbz-PN being similar at 15 and 12%, respectively. These results indicate that these compounds are not efficient fluorophores. With oxygen purging, 2Cbz-PN displays a slight enhancement in $\Phi_{\rm F}$, increasing to 21%. However, the Φ_F of both BFCbz-PN and BTCbz-PN nearly double to 28 and 24%, respectively, after oxygen purging. Such enhancements have traditionally been attributed to the TADF mechanism, the reasoning being that the enhancement is due to the newly unquenched triplet states undergoing rISC. However, it is worth noting that the phosphorescence spectra of the investigated compounds display a large degree of overlap with the fluorescence spectra. 23,24 Thus it is possible that the observed $\Phi_{\rm F}$ enhancements of the PN-acceptor compounds could be due to enhanced rare room-temperature phosphorescence. As such,

 Φ_F enhancement is a good indicator that the triplet state is utilized in the emissive mechanism but should not be used as the sole metric to indicate TADF activity for these compounds.

3.3. Two-Photon Absorption. The two-photon induced emission and TPA cross sections were obtained to gain insight into the CT character of these emitters. This is because the TPA transition probability increases with increasing ICT character. The two-photon induced emission of the investigated chromophores is displayed in Figure 5 and is in good agreement with the steady-state fluorescence spectra. A red shift in the two-photon emission spectra is observed for BFCbz-Trz and BTCbz-Trz relative to that of Cbz-Trz. A similar trend is observed for the PN-acceptor compounds, with BFCbz-PN and BTCbz-PN emissions being red-shifted from that of 2Cbz-PN.

Logarithmic plots of counts per second of two-photon induced emission versus beam power (mW) were constructed for each sample and are displayed as insets in Figure 5. These plots gave a linear fit with a positive slope of approximately 2 for all samples, confirming the TPA process. The TPA cross-section values are displayed in Table 1. Cbz-Trz has a relatively low cross-section value of 1.01 GM. This value was greatly enhanced to 14.9 and 8.8 GM, respectively, when BF or BT is the donor moiety. This finding confirms that BF and BT provide greater donor contribution than the carbazole unit, which is in agreement with previous studies that relate donor—acceptor strength to CT character. 21,57

2Cbz-PN has a TPA cross section of 15.9 GM, much higher than that of Cbz-Trz. This indicates that the combination of PN-acceptor and carbazole donor leads to greater ICT character. BTCbz-PN has a TPA cross section of 21.8 GM, indicating that increasing the donor strength of the compound does increase its ICT character. This is in good agreement with the steady-state measurements. The TPA cross section is enhanced to 44.4 GM with the BF donor. This is likely because of the oxygen in the molecular structure being a better electron-withdrawing group, increasing the ICT character even further. The order of increasing ICT character is consistent between both the Trz- and PN-acceptor compounds, where the compound with the BF donor displays the greatest ICT characteristics.

3.4. Time-Resolved Fluorescence Up-Conversion. Fluorescence decay measurements were conducted on all compounds in unpurged toluene. Purged solutions were not able to be tested due to limitations of the fluorescence upconversion sample holder. Two decay components were observed for the Trz-acceptor compounds, with each component displaying different lifetimes (Table 2). These decay traces (Figure 6) were each fitted to a double exponential decay function, yielding an initial decay for the

Table 2. Up-Conversion Emissive Lifetime Values of Investigated Compounds in Unpurged Toluene

compound	$ au_1 ext{ (ps)}$	τ_2 (ps)	τ_3 (ps)
Cbz-Trz	149	>2200	0
BFCbz-Trz	162	>2200	0
BTCbz-Trz	114	>2200	0
2Cbz-PN	4	31	>2200
BFCbz-PN	5	40	>2200
BTCbz-PN	4	64	>2200

first component of 114–160 ps and a longer decay that exceeded 2 ns for the second component.

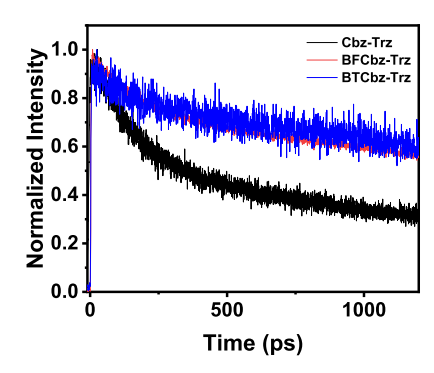
The decay profiles of the PN-acceptor compounds display dynamics different from those of the Trz-acceptor compounds. Here, we observe three decay components, each with a different lifetime. The decay trace was fitted using a three-exponential decay function, yielding a very fast initial decay (<7 ps), a fast second decay (30–60 ps), and a relatively long-lived final decay (>2 ns). The first component is of particular interest as it is consistent across all PN-acceptor compounds and is absent for the Trz-acceptor compounds. Thus, this component is likely tied to the molecular structure of the PN-acceptor compounds.

One possible explanation is that the PN-acceptor compounds have faster and more efficient CT, going from a delocalized state to a localized state, due to their donor units being directly linked to the acceptor. The differences between the emissive dynamics of the Trz- and PN-acceptors could also be due to how the two classes of compounds interact with the solvent toluene. This would indicate that the CT characteristics of the two classes are significantly different as the solvent polarity is known to alter emissive properties. As the decay of the longest component continues past the limit of detection for this system, the TCSPC technique is utilized to further investigate the emissive dynamics of these compounds.

3.5. TCSPC. To better understand the emissive dynamics of the investigated compounds, the emissive lifetimes were obtained using the TCSPC technique. As all Trz-acceptor compounds display similar emissive dynamics, only the results for BFCbz-Trz are shown here. For similar reasons, only the results of BFCbz-PN are displayed here. The emission traces of BFCbz-Trz and BFCbz-PN are displayed in Figure 7, while the results for all other investigated compounds are provided in the Supporting Information (Figure S1). The emissive lifetimes of all investigated compounds are displayed in Table 3. The purged measurements were conducted to determine as to what extent the triplet state is involved in the emissive mechanism. The understanding being that if the triplet state plays a role in emission, a long-lived emissive component should be observed. As oxygen is known to quench triplet states, an increase in the lifetime of the aforementioned long-lived component should be observed with oxygen purging.^{3,52,63,64}

We immediately observe that the traces for BFCbz-Trz and BFCbz-PN are substantially different, an observation that is consistent with the other PN-acceptor compounds and their Trz-acceptor counterparts (Figure S1). Cbz-Trz has an emissive lifetime of 4.6 ns that is only slightly enhanced with purging to 5.3 ns. There is little change in the emissive lifetime when BF or BT is used as the donor. BFCbz-Trz and BTCbz-Trz have emissive lifetimes of 4.8 and 4.2 ns that are only slightly enhanced with purging to 5.6 and 4.9 ns, respectively. These findings reveal that the Trz-acceptor compounds all have emissive lifetimes typical of fluorescent emitters.³ The inset of Figure 7 reveals that BFCbz-Trz lacks a long-lived emissive component that would indicate that triplet states play a role in the emissive mechanism. Cbz-Trz and BTCbz-Trz also lack this component (Figure S1). This observation indicates that triplet states do not play a substantial role in the emissive process. However, the results suggest that triplet states play an emissive role for the PN-acceptor compounds.

The inset of Figure 7 reveals that BFCbz-PN has two fluorescent components. These two components were also



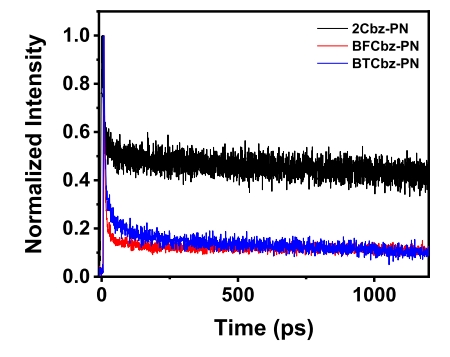


Figure 6. Time-resolved fluorescence up-conversion results of the Trz-acceptor compounds (left) and the PN-acceptor compounds (right) in toluene.

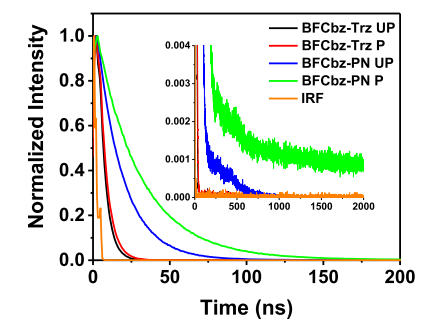


Figure 7. TCSPC measurements of BFCbz-Trz and BFCbz-PN in unpurged and purged toluene solutions. Inset is a zoom-in of the emission lifetime.

Table 3. Lifetimes of the Components of Fluorescence in Toluene Solutions

T_{short} unpurged/purged (ns)	T_{long} unpurged/purged (ns)
4.6/5.3	0/0
4.8/5.6	0/0
4.2/4.9	0/0
19/30	223/1247
24/39	196/2090
23/38	201/1980
	4.6/5.3 4.8/5.6 4.2/4.9 19/30 24/39

observed for 2Cbz-PN and BTCbz-PN (Figure S1). The first component of 2Cbz-PN is rather short-lived compared to the second component, having a lifetime of 19 ns, which is enhanced to 30 ns with oxygen purging. The replacement of the carbazole donor with BF or BT only slightly enhances the first component lifetime to 24 and 23 ns for BFCbz-PN and BTCbz-PN in unpurged toluene, respectively. These short-lived components are enhanced with oxygen purging, increasing to lifetimes of 39 ns for BFCbz-PN and 38 ns for BTCbz-PN. These lifetimes are significantly greater than those of the Trz-acceptor compounds, indicating that they are comparatively less efficient fluorophores.

The second emissive component displays a much more pronounced enhancement with the removal of oxygen (Figure S2). This is clearly observed for 2Cbz-PN, where the second component lifetime increases from 223 to 1247 ns with oxygen purging. The enhancement observed for BFCbz-PN and BTCbz-PN was even more drastic, increasing from 196 to 2090 and 201 to 1980 ns, respectively. The presence of a long-lived emissive component that is altered by the presence of oxygen indicates that there is some emissive mechanism that utilized triplet states in the same wavelength region as singlet

emission. The prompt component decay has been attributed to a decay process that primarily utilizes the singlet excited state due to its lifetime being only slightly altered by oxygen purging. The long-lived component has been attributed to a decay process that primarily relies on the triplet excited state.

3.6. nsTAS. The nsTAS technique was utilized to investigate the decay lifetimes of both the emissive and nonemissive transient species of the chromophores. These species are observed as either a negative or positive change in optical absorption (Δ OD) and are the result of ground state bleach (GSB), spontaneous emission (SE), or excited state absorption (ESA). The lifetimes of these peaks provide information for determining the character of the transient species and the emissive mechanism. The transient absorption spectra for each of the Trz-acceptor and PN-acceptor compounds display dynamics similar to those of BFCbz-Trz and BFCbz-PN, respectively. As such, only BFCbz-Trz and BFCbz-PN are discussed here. Their transient absorption spectra are displayed in Figures 8 and 9, while the transient absorption spectra of the other compounds are provided in the Supporting Information (Figures S3 and S4).

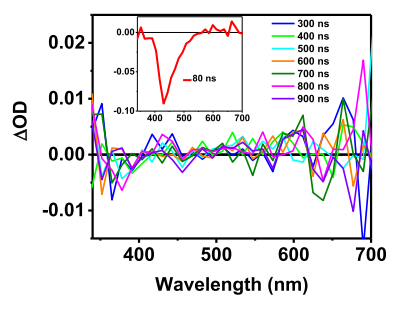


Figure 8. nsTAS of BFCbz-Trz in purged toluene. The inset displays the SE peak at 80 ns.

The nsTAS mapping of BFCbz-Trz reveals a large SE peak that has a maximum at the same wavelength as the steady-state fluorescence. There is also a short-lived GSB within the same region as the steady-state absorption. There appears to be ESA peaks at 350 and 650 nm. However, the kinetic traces taken at these wavelengths (Figure S5) reveal that these peaks are only noise. The kinetic traces of the other Trz-acceptor compounds yielded similar results. Thus, it is determined that no long-lived ESAs are observed for any of the other Trz-acceptor compounds. This result further supports that these emitters utilize fluorescence and do not utilize the triplet state for emission.

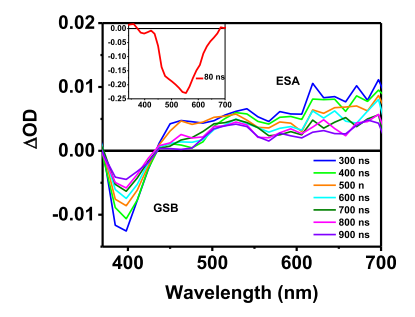


Figure 9. nsTAS of BFCbz-PN in purged toluene. The inset displays the SE peak at 80 ns.

The transient absorption spectrum for BFCbz-PN reveals excited-state dynamics that are quite different from that for BFCbz-Trz. First, a GSB is observed at 400 nm and is attributed to depletion of the ground state and overlaps with the ICT transition observed in the steady-state absorbance spectrum. This is followed by a large SE peak, attributed to fluorescence. Unlike BFCbz-Trz, there is ESA that is within the same region as the emission and is able to be resolved due to the time delay of the nsTAS technique. This ESA is a long-lived state that displays sensitivity to oxygen in solution and is present in the transient absorption spectra of each of the PN-acceptor compounds. The ESA and GSB kinetic traces for BFCbz-PN are displayed in Figure 10, with the kinetic traces of

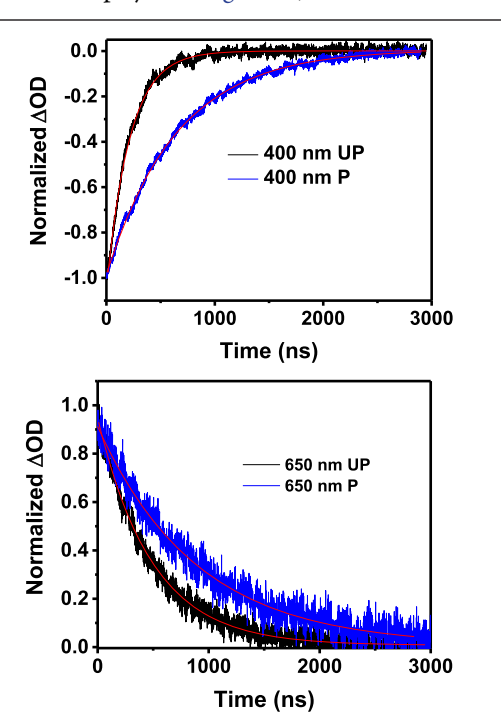


Figure 10. GSB (top) and ESA (bottom) decays of BFCbz-PN in unpurged and purged toluene solutions. The red lines represent the monoexponential decay fittings.

the other PN-acceptor compounds available in the Supporting Information (Figures S6 and S7). Decay lifetimes of these states in unpurged and purged solutions are displayed in Table 4. The decay dynamics of each PN-acceptor compound is similar, so only the dynamics BFCbz-PN will be described here. The GSB displays a lifetime of 230 ns that is enhanced to 652 ns with oxygen purging. This is expected as the various triplet ESAs provide significant contribution to the GSB lifetime. The ESA lifetime is 488 ns in unpurged solution and is enhanced to 929 ns with oxygen purging. This supports the characterization of ESA as a triplet state.

The ESA decay values obtained from nsTAS were utilized to calculate $k_{\rm rISC}$. The $k_{\rm rISC}$ values, displayed in Table 4, for each PN-acceptor compound were approximated utilizing the previously described Vázquez and Masui methods. ^{11,14} While there is disagreement between the obtained values, the trend within the values is consistent. 2Cbz-PN has the lowest $k_{\rm rISC}$, indicating that it is the least efficient TADF emitter among the PN-acceptor compounds. BFCbz-PN and BTCbz-PN have similar efficiencies, regardless of which calculation method is used. It is worth noting that the method developed by Vázquez et al. displays the same trend in efficiencies that was observed in previous studies. ²⁴ We would like to reiterate that no ESAs were observed for the Trz-acceptor compounds. As such, no ESA decay kinetics nor subsequent $k_{\rm rISC}$ values were obtained for the Trz-acceptor compounds.

3.7. Quantum Chemical Simulations. In order to establish a connection between the molecular structure and the observed photophysical properties, with a focus on the influence of the phenylene linker, quantum chemical calculations were conducted on all Trz- and PN-acceptor compounds based on the structures displayed in Figure 2. As the computational results for each of the Trz- and PN-acceptor compounds are similar to BFCbz-Trz and BFCbz-PN, respectively, only BFCbz-Trz and BFCbz-PN are discussed here. The computational results for all other compounds are displayed in the Supporting Information.

Optimized ground-state geometries were obtained for each compound to investigate the influence of the phenylene bridge on the dihedral angle (Figures 11 and S8). Our results show that the inclusion of the linker causes the dihedral angle to remain relatively the same, regardless of which donor unit is used. The Trz-acceptor compounds have strikingly similar dihedral angles, where the ground-state dihedral angles of Cbz-Trz, BFCbz-Trz, and BTCbz-Trz are 54.3, 53.4, and 54.5°, respectively. These results are interesting as it was expected that the bulkier BF and BT donor units would cause an appreciable increase in the dihedral angle. A likely reason for each Trz-acceptor compound having similar ground-state dihedral angles is that there is little steric hindrance due to the linear structure of the Trz-acceptor compounds. Thus, the dihedral angle of the Trz-acceptor compounds does not change much, even with the use of BF or BT as donors (Table 5).

Table 4. Decay Lifetimes of the Transient States of PN-Acceptor Compounds in Unpurged and Purged Toluene^a

compound	$ au_{ m GSB}$ UP(ns)	$ au_{GSB}$ P(ns)	$ au_{ESA}$ UP(ns)	$ au_{ESA} P(ns)$	$k_{\rm ESA}~(\rm s^{-1})$	$k_{\rm rISC}~({\rm s}^{-1})~{\rm V\'azquez}^{16}$	$k_{\rm rISC}~({\rm s}^{-1})~{\rm Masui}^{11,14}$
2Cbz-PN	307	695	325	775	1.29×10^{6}	5.16×10^4	8.51×10^{3}
BFCbz-PN	221	655	488	871	1.15×10^{6}	1.49×10^{5}	1.40×10^4
BTCbz-PN	217	585	208	856	1.17×10^{6}	1.40×10^{5}	1.54×10^4

^aAlso included are k_{rISC} values using two different methods.

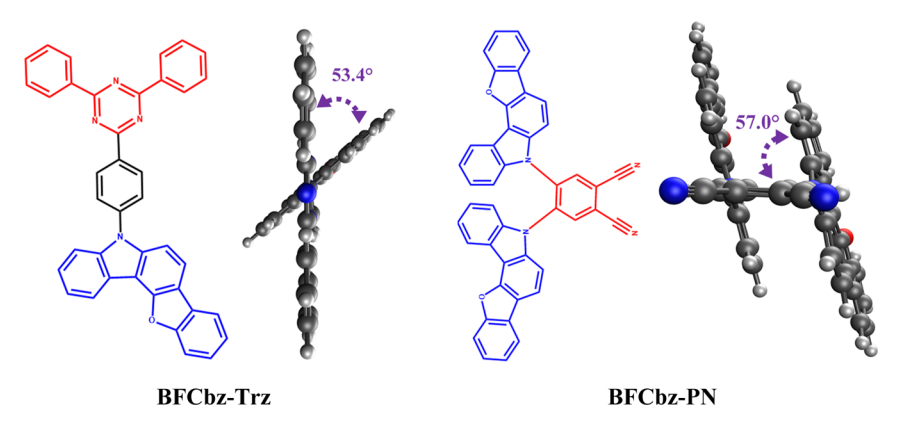


Figure 11. Optimized ground state (from ωB97X-D) dihedral angles of BFCbz-Trz and BFCbz-PN.

Table 5. Quantum Chemical Results for Investigated Compounds, along with Experimental and Calculated k_{rISC}

compound	$\frac{\Delta E_{\mathrm{ST}}}{(\mathrm{eV})}$	V _{SOC} (eV)	$k_{ m rISC} \ { m P} \ ({ m s}^{-1}) \ { m Vazquez}^{16}$	$\text{TD-DFT}_{(s^{-1})} k_{\text{rISC}}$
Cbz-Trz	1.00	1.3×10^{-3}	0/0	5.5×10^{-10}
BFCbz-Trz	0.93	1.3×10^{-3}	0/0	1.1×10^{-7}
BTCbz-Trz	0.95	1.3×10^{-3}	0/0	2.1×10^{-8}
2Cbz-PN	0.53	1.5×10^{-4}	5.16×10^4	1.1×10^{-1}
BFCbz-PN	0.37	1.3×10^{-4}	1.49×10^{5}	9.3×10^{1}
BTCbz-PN	0.38	1.3×10^{-4}	1.40×10^{5}	3.8×10^{1}

As the molecular structure of PN-acceptor compounds does not include a linker, the use of BF or BT as donor units has a greater influence on their dihedral angles. We observe this as 2Cbz-PN has a ground-state dihedral angle of 49.5°, which is increased to 57.0 and 57.2° for BFCbz-PN and BTCbz-PN, respectively. This increase is attributed to the branched molecular structure of the PN-acceptor compounds, which induces steric hindrance between the two donor groups. Because BF and BT are bulkier than carbazole, steric hindrance between the two donors is increased leading to larger dihedral angles. It is interesting that there is little difference between the dihedral angles of the BF or BT derivatives. This slight difference suggests that the heteroatom plays only a small role in the ground-state dihedral angles, with the molecular structure and size of the donor group having the most significant contribution. When comparing the optimized ground state to the optimized excited singlet and triplet geometries of the Trz- and PN-acceptor chromophores, there are differences in dihedral angles due to the chromophores being in the relaxed versus excited state. However, the trends observed for the ground-state geometries are also seen in the excited-state geometries (Table S1).

The NTOs of the Trz- and PN-acceptor chromophores were obtained to further elucidate the influence of molecular structure on CT character and HOMO/LUMO separation (Figures 12 and S9). Each compound has some degree of CT character, and it can be seen in the transition from the ground state to the excited singlet state ($S_0 \rightarrow S_1$). The Trz-acceptor compounds have limited separation of the exciton NTO (HOMO) and hole NTO (LUMO). The HOMO is largely localized on the donor unit and the phenylene bridge connecting the donor and the diphenyltriazine acceptor. The LUMO is localized on the phenylene bridge and the Trz ring of the acceptor unit. Some electron density of the LUMO remains on the donor unit, with none present on the phenyl

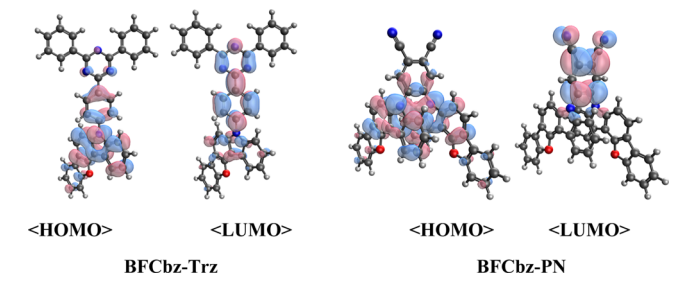


Figure 12. NTOs (from ω B97X-D) for CT states of BFCbz-Trz and BFCbz-PN.

rings of the Trz-acceptor. Such a large degree of HOMO/LUMO overlap suggests that the phenylene bridge inhibits HOMO/LUMO separation when only one donor unit is used.

Due to their donor and acceptor units being directly linked, most of the PN-acceptor compounds display substantial HOMO/LUMO separation. For 2Cbz-PN, the HOMO is localized on the two carbazole donors and the ring of the PNacceptor. The LUMO has significant overlap with the HOMO, being localized almost entirely on the acceptor, with some electron density on the two donors (Figure S9). HOMO/ LUMO separation is increased with the use of BF as the donor group, where the HOMO is mostly localized on the two donors, while the localization of the LUMO is largely unaffected (Figure 12). For both the Trz- and PN-acceptor compounds, no significant differences in HOMO/LUMO separation are observed between using BF or BT as the donor unit. These results indicate that increasing the donor strength increases HOMO/LUMO separation, provided that the donor and the acceptor are directly linked without the use of a bridge.

The adiabatic energy gaps between the excited singlet and excited triplet states ($\Delta E_{\rm ST}$) and SOC constants ($V_{\rm SOC}$) were calculated to determine $k_{\rm rISC}$ for the investigated compounds (Table 5). The trends and differences observed for dihedral angles and HOMO/LUMO separation are also observed for ($\Delta E_{\rm ST}$) and $k_{\rm rISC}$. We observe that $\Delta E_{\rm ST}$ for BFCbz-Trz (0.93 eV) is significantly larger (~3×) than that of BFCbz-PN (0.37 eV) (Figure S10). Similar results were obtained for the remaining Trz- and PN-acceptor compounds. The calculated $k_{\rm rISC}$ of BFCbz-Trz and BFCbz-PN, 1.1 × 10⁻⁷ and 9.3 × 10¹, respectively, suggests that only the PN-acceptor compounds are capable of undergoing rISC. This result suggests a correlation between $\Delta E_{\rm ST}$ and $k_{\rm rISC}$, where $k_{\rm rISC}$ decreases as $\Delta E_{\rm ST}$ increases. This finding is in agreement with the current understanding of the TADF mechanism. ¹³ Based on these

results, the PN-acceptor compounds have a significantly greater chance of undergoing rISC and achieving TADF than their Trz-acceptor counterparts. These results also indicate that both BFCbz-PN and BTCbz-PN are more efficient TADF emitters than 2Cbz-PN, consistent with previous reports. This is associated with their smaller $\Delta E_{\rm ST}$ and higher degree of HOMO/LUMO separation. This is also reflected in the results of the previously discussed optical measurements. Of the PN-acceptor compounds, BFCbz-PN has a slightly more efficient TADF mechanism due to its smaller $\Delta E_{\rm ST}$ and higher electronegative heteroatom. This result is again consistent with previous reports. The previous reports are significantly greater than the previous reports.

4. DISCUSSION

In this report, we utilize high-resolution, steady-state, time-resolved, and nonlinear optical spectroscopic techniques as well as quantum chemical calculations to investigate the photophysical properties of carbazole-based emitters. Our measurements reveal stark differences in the emissive mechanism between the Trz- and PN-acceptor compounds. These differences are based on the molecular structure, namely, the presence or absence of the phenylene linker. To aid in the clarity of this section, the Trz-acceptor compounds are discussed first followed by the PN-acceptor compounds.

The steady-state measurements reveal that the Trz-acceptor compounds have an extremely high $\Phi_{\rm F}$ (>90%) that displays a slight enhancement when oxygen is purged from solution. This enhancement could indicate that triplet states play a role in their emissive mechanism. However, such high Φ_F in unpurged solution indicates that $k_{\rm F}$ is so efficient that it heavily outcompetes the rates of other singlet decay pathways including k_{nr} and k_{ISC} . In addition to this, oxygen has also been observed to quench singlet states.⁵² Thus, emissive lifetime measurements were conducted to aid in determining the role of excited triplets in the emissive mechanism. These measurements reveal that Trz-acceptor compounds have emissive lifetimes of ~5 ns which is largely unaffected by oxygen purging. Long-lived emissive components, which would indicate emission that relies on excited triplets, were not observed for any of the Trz-acceptor compounds.³ This matches expectations as it would be unusual to observe a longlived emissive component for compounds with such a high $\Phi_{\rm E}$. This expectation arises from the understanding that the longer the lifetime of the excited states, the greater the chance that they will be quenched by a nonradiative process. The nsTAS results support this as no triplet states are observed in the transient absorption spectra for these compounds. This is significant as some triplet states should be observed if $k_{\rm ISC}$ was able to compete with k_F . A likely cause for low $k_{\rm ISC}$ is the relatively high singlet-triplet energy gap for these compounds (0.93-1.0 eV). Such a large gap impedes SOC which is required for ISC. Due to these factors, $k_{\rm F}$ is able to substantially outcompete $k_{\rm ISC}$, and the observed $\Phi_{\rm F}$ enhancement is determined to be the result of newly unquenched singlet states.

The substantial Φ_F of the Trz-acceptor compounds is also the result of the phenylene linker. It was expected that a significant amount energy would be dissipated via molecular motion, thus impacting Φ_F . However, the quantum chemical calculations reveal that this is not the case. The dihedral angles between the donor and the phenylene linker (Table S1) show that there is little difference between the ground- and excited-state dihedral angles (\sim 2°). These results indicate that only a

small portion of energy is lost to molecular motion. The likely cause for such a small change in the dihedral angle is that by physically separating the donor and acceptor units, such as via a phenylene linker, electron repulsion is reduced, thus diminishing the dihedral angle.

The phenylene linker also affects the HOMO/LUMO separation, as shown by the NTO results. For each Trzacceptor compound, the HOMO is localized on the donor and phenylene linker, while the LUMO is mostly centered on the phenylene linker and the central ring of the Trz-acceptor. It appears that the dual phenyl rings of the acceptor unit do not provide significant contribution as electron withdrawers. A particularly interesting observation is that the stronger BF and BT donors reduce HOMO/LUMO separation, causing some of the LUMO to be on the donor unit. As significant separation is considered to be a requirement for TADF activity, it is little wonder that these compounds do not display any of the characteristics commonly associated with the TADF process. 1,2,11,22 The $\Delta E_{\rm ST}$ of these compounds are also relatively large, being significantly greater than the reported energy required for rISC to take place (Table 4). 4,17 It appears that having the donor and acceptor connected via a bridge does not aid in HOMO/LUMO separation as both HOMO and LUMO densities of these compounds are partially localized on the phenylene linker.

The steady-state measurements show that the PN-acceptor compounds have significantly lower Φ_F than the Trz-acceptor compounds. Such Φ_F indicates that other processes that deplete the singlet excited state, such as $k_{\rm ISC}$, take place for these compounds. These compounds also display significantly larger enhancements when oxygen is purged from the solution than the Trz-acceptor compounds. As stated previously, this could indicate that these compounds utilize the triplet state for emission. The up-conversion results reveal that 2Cbz-PN has a more complex emissive decay process than Cbz-Trz. We observe three components, with the third and last component having an extremely long lifetime. The third component has the greatest contribution to the emission. However, similar to Cbz-Trz, the total lifetime was not able to be resolved by the time-resolved fluorescence up-conversion technique. Thus, the TCSPC technique was again used to fully resolve the emissive lifetime. The TCSPC technique was also used to further determine to what degree the triplet state plays a role in emission. It is apparent that the PN-acceptor compounds have two emissive components on the ns timescale. However, the second emissive component could be the result of phosphorescence that overlaps with the fluorescence spectrum. This could be the reason for it having such low intensity when compared to the first component as room-temperature phosphorescence is not expected to be very intense. Instead, our focus is on the first emissive component as it displays some interesting dynamics.

The lifetime of the first emissive component is nearly 6–7 times longer than those of the Trz-acceptor compounds. This supports the determination that $k_{\rm F}$ is not as efficient for the PN-acceptor compounds as this longer lifetime indicates a diminished $k_{\rm F}$, consistent with $\Phi_{\rm F}$ results. Also consistent with $\Phi_{\rm F}$ results, the first component lifetime is significantly enhanced with oxygen purging. This was unexpected as the emissive trace for the Trz-acceptor compounds, which is also determined to be from fluorescence, shows little enhancement with oxygen purging. The observation of two emissive components, with the second component being long-lived, is

often associated with the TADF process.^{23,65} However, it was expected that emission from TADF emitters would have a similar lifetime as emission from fluorescent compounds. This expectation arises from the understanding that rISC results in emission from the singlet state. Such an emission should display similar dynamics as typical fluorescence. Here, it is important to note that the phosphorescence spectra of each of the PN-acceptor compounds have a high degree of overlap with the fluorescence spectra. 11,24 The overlap is such that at the fluorescence peak, which the TCSPC detector is set to, there is possibly some phosphorescence activity. If emission from both singlet and triplet states occurs at the same wavelength, as is the case with these compounds, the TCSPC technique cannot distinguish between the two. This means that the observed long-lived emissive component could be the result of phosphorescence. However, room-temperature phosphorescence is expected to be an inefficient process for organic compounds. This could explain why the long-lived emissive component has such low signal when compared to the short-lived first component. Thus, TCSPC is not used to definitively determine TADF activity, and more thorough investigation utilizing nsTAS is conducted.

Similar to the report by He et al., 21 a large SE peak was observed in the same region as the ESA peaks. These peaks were able to be resolved due to the time delay of the nsTAS technique. It was confirmed that these peaks were above the noise level and are triplet excited states for the PN-acceptor compounds. The broadness of the ESA peaks indicates that the PN-acceptor compounds are able to populate triplet states of various energies. 13 As expected, the lifetime of the triplet state is enhanced with oxygen purging. Analysis of τ_{ESA} , k_{ESA} , and $k_{ ext{rISC}}$ reveals a connection between the triplet state and the $\Phi_{ ext{F}}$ and emissive lifetimes. 2Cbz-PN has the longest ESA lifetime, lowest k_{ESA} , and lowest k_{rISC} . These characteristics indicate that processes that deplete the triplet state, including k_{rISC} , are inefficient for this compound. This is one cause for 2Cbz-PN displaying a smaller Φ_F enhancement when compared to BFCbz-PN and BTCbz-PN. However, BFCbz-PN and BTCbz-PN have shorter ESA lifetimes and more efficient $k_{\rm ESA}$ and $k_{\rm rISC}$. This result follows the same trend as their greater $\Phi_{\rm F}$ enhancement and longer emissive component lifetimes. It is thus determined that the PN-acceptor compounds utilize the triplet states in a rISC process. The TPA and quantum chemical calculations aid in understanding the structurefunction relationship for the observed excited-state and emissive dynamics.

The lack of a phenylene linker in the PN-acceptor molecular design results in characteristics very different from what was observed for the Trz-acceptor compounds. First, the larger TPA cross section of the PN-acceptor compounds indicate that they have greater CT character than the Trz-acceptor compounds. This comes from the understanding that stronger donors increase the CT character, thus enhancing the transition moment of TPA. 53,54,56

This interpretation of the TPA cross-section results is supported by the quantum chemical calculations, which reveal that the PN-acceptor compounds also have a greater degree of HOMO/LUMO separation than the Trz-acceptor compounds. 2Cbz-PN has its HOMO localized on the two carbazole donors and the ring of the PN-acceptor, with the LUMO being localized almost completely on the entire acceptor unit. This localization indicates that the PN-acceptor acts as an efficient electron-withdrawing group, aiding in HOMO/LUMO sepa-

ration. This separation is enhanced with the use of BF or BT as donor groups, where the HOMOs of BFCbz-PN and BTCbz-PN are completely localized on the donor units. The LUMO is largely unaffected, still being somewhat present on the donor units, which maintains the partial overlap required for TADF. Interestingly, there is little difference in HOMO/LUMO separation between BFCbz-PN and BTCbz-PN, indicating that different heteroatoms play only a small role in this. The ΔE_{ST} of these compounds is also significantly smaller than their Trzcounterparts. This small $\Delta E_{\rm ST}$ allows for greater SOC between the singlet and triplet manifolds and an enhanced $k_{\rm rISC}$. $\Delta E_{\rm ST}$ of the BF and BT derivatives are smaller than that of 2Cbz-PN (Table 4). This is likely due to the HOMO/LUMO energy gap of the BF and BT donor units being smaller than that of carbazole. 1,66,67 The greater HOMO/LUMO separation observed for the PN-acceptor compounds has been attributed to two factors: (1) the donors are directly linked to the acceptor unit and (2) there are two donor units that further contribute to the overall donor strength. All of these factors contribute to the PN-acceptor compounds demonstrating TADF properties.

Two experimental methods and quantum chemical calculations were utilized to approximate k_{rISC} for all investigated compounds. No k_{rISC} values for the Trz-acceptor compounds could be determined using either experimental method due to no long-lived emissive component or triplet states being observed. However, using quantum chemical calculations, k_{rISC} values on the order of 10^{-7} to 10^{-10} were obtained for the Trzacceptor compounds. These values indicate that the rISC process is unlikely to occur in these compounds, which is consistent with all experimental results. All methods of calculation indicate that the rISC process is accessible to the PN-acceptor compounds. While there is disagreement in the actual values, as is to be expected, the trend is clear. Both BFCbz-PN and BTCbz-PN display greater k_{rISC} than 2Cbz-PN, indicating that increasing donor contribution enhances TADF activity. Our results display a clear correlation between molecular design and TADF activity, where the PN-acceptor compounds are TADF-active, while the Trz-acceptor compounds are not. This is reflected in the external quantum efficiencies (EQEs) of OLEDs fabricated with these compounds as emitters.

Devices that utilize the PN-acceptor compounds as emitters generally have better performance than those that utilize Trz-acceptor compounds. ^{24,68} At 10 wt % and DPEPO as the host, an OLED using Cbz-Trz as the emitter achieved an EQE of 4.2%.68 However, using mCP as the host and only 1 wt % 2Cbz-PN, a device was fabricated that had an EQE of 7%.²⁴ Under identical device parameters and using BFCbz-PN or BTCbz-PN as the emitter, the EQE is almost doubled to ~12%.24 Based on our time-resolved, steady-state, and quantum chemical simulations, we assert that the PN-acceptor compounds are TADF-active emitters, while the Trz-acceptor compounds are not. However, our results do not fully agree with the reported device properties of BFCbz-Trz, where at 10 wt % in DPEPO, many of the characteristics associated with TADF were observed.²³ This raises two questions: (1) why is the TADF effect observed for BFCbz-Trz and not Cbz-Trz and (2) why are TADF characteristics observed for BFCbz-Trz in solid-state but not in solution.

Regarding the first question, it is important to note that all device parameters of the Cbz-Trz and BFCbz-Trz OLEDs are identical, save the emissive layer. ^{23,68} This indicates that the

differences in device properties are related to this layer. Thus, any differences between the two OLEDs can be attributed to the different donor unit of the emitter, either carbazole or BF. It is likely that BFCbz-Trz has guest—host interactions that induce the TADF characteristics due to its donor unit. More in-depth studies are needed to determine what these interactions are and how they can be utilized to improve the device EQE.

Regarding the second question, the interactions between guest and host materials are still not well understood. However, it is well established that the device properties can be dramatically altered depending on the wt % of emitter used and the choice of host material. 11,23,24,69,70 One proposed explanation for guest-host interactions has been described as solid-state solvation, where the properties of the host matrix, such as polarity, can alter the emissive properties of the embedded chromophore. 61,62 From the TPA results, we determined that BFCbz-Trz has the greatest CT character of the Trz-acceptor compounds. This indicates that it would be most affected by host polarity and the energy levels of its singlet and triplet excited states being greatly diminished in polar hosts such as DPEPO. If this is the case, then it is perhaps possible to induce the TADF mechanism by utilizing the correct guest-host blend. This assertion is supported by the different device properties obtained for Cbz-Trz and BFCbz-Trz, where the only difference in the emissive layer was the emitter itself. Determining the exact parameters that would match a host and emitter to induce the TADF mechanism would require its own in-depth investigation and would likely be time-consuming. Thus, it is more favorable to begin TADFbased OLED design and fabrication with an emitter that displays TADF characteristics in solution and free of guesthost interactions.

5. CONCLUSIONS

Our study has revealed that despite both classes of compounds being designed to be TADF-active compounds, the Trz- and PN-acceptor compounds display very different excited-state dynamics in solution. The Trz-acceptor compounds display only one of the characteristics expected of a TADF emitter, that being $\Phi_{\rm F}$ enhancement with oxygen purging. However, they have short emissive lifetimes and lack an ESA which could be associated with triplet states. Due to the lack of these components, no $k_{\rm rISC}$ values could be determined for these compounds with our experimental methods. Thus, the Trz-acceptor compounds are determined to be TADF-inactive materials.

Unlike their Trz-counterparts, each of the PN-acceptor compounds display all of the characteristics traditionally associated with the TADF process. They have relatively small $\Phi_{\rm F}$ values which are enhanced with oxygen purging. This, in addition to a long emissive lifetime, indicates that $k_{\rm F}$ is not as efficient for these compounds, allowing for other decay pathways to utilize the excited states. Their transient absorption spectra reveal long-lived triplet states which could undergo various decay pathways, including rISC. Using experimental methods and quantum chemical calculations, $k_{\rm rISC}$ was approximated for these compounds, which indicate that rISC is a viable pathway for each PN-acceptor compound. Thus, it was determined that these compounds are TADF-active emitters.

Structure-function relationships were also established, where the observed photophysics of the PN-acceptor

compounds is the result of directly linking the donor to the acceptor unit. This molecular design induces sufficient HOMO/LUMO separation, small $\Delta E_{\rm ST}$, and enhanced $V_{\rm SOC}$ between the triplet and singlet manifolds. By increasing the donor strength, that is, using BF or BT as donors instead of carbazole, each of these factors is enhanced, which in turn enhances $k_{\rm rISC}$. This finding indicates that sufficient donor contribution is required for TADF activity. It is our hope that our results can improve the design principles of TADF compounds and highlight the importance of considering guest—host interactions for future measurements.

ASSOCIATED CONTENT

Supporting Information

The Supporting Information is available free of charge at https://pubs.acs.org/doi/10.1021/acs.chemmater.1c03668.

TCSPC, nsTAS, GSB and excited-state decay kinetics, and formulas for determining $\Delta E_{\rm ST}$, $V_{\rm SOC}$, and $k_{\rm rISC}$ via quantum chemical simulations (PDF)

AUTHOR INFORMATION

Corresponding Author

Theodore Goodson, III — Department of Chemistry, University of Michigan, Ann Arbor, Michigan 48109, United States; orcid.org/0000-0003-2453-2290; Email: tgoodson@umich.edu

Authors

Lloyd Fisher, Jr. — Department of Chemistry, University of Michigan, Ann Arbor, Michigan 48109, United States;
orcid.org/0000-0002-6792-7199

Ricardo Javier Vázquez — Department of Chemistry, University of Michigan, Ann Arbor, Michigan 48109, United States; orcid.org/0000-0003-3245-8123

Madeleine Howell – Department of Chemistry, University of Michigan, Ann Arbor, Michigan 48109, United States

Angelar K. Muthike – Department of Chemistry, University of Michigan, Ann Arbor, Michigan 48109, United States

Meghan E. Orr – Department of Chemistry, University of Michigan, Ann Arbor, Michigan 48109, United States

 Hanjie Jiang – Department of Chemistry, University of Michigan, Ann Arbor, Michigan 48109, United States

Betsy Dodgen – Department of Chemistry, University of Michigan, Ann Arbor, Michigan 48109, United States

Dong Ryun Lee – School of Chemical and Engineering, Sunkyunkwan University, Suwon-si, Gyeonggi-do 446-740, Republic of Korea

Jun Yeob Lee — School of Chemical and Engineering, Sunkyunkwan University, Suwon-si, Gyeonggi-do 446-740, Republic of Korea; orcid.org/0000-0002-7677-0605

Paul Zimmerman – Department of Chemistry, University of Michigan, Ann Arbor, Michigan 48109, United States;
o orcid.org/0000-0002-7444-1314

Complete contact information is available at: https://pubs.acs.org/10.1021/acs.chemmater.1c03668

Notes

The authors declare no competing financial interest.

ACKNOWLEDGMENTS

T.G. III acknowledges support from the US Air Force Office of Scientific Research in the Biophysics Program via grant

FA9550-20-1-0380 and from the National Science Foundation through grant CHE2004076.

REFERENCES

- (1) Samanta, P. K.; Kim, D.; Coropceanu, V.; Brédas, J.-L. Up-Conversion Intersystem Crossing Rates in Organic Emitters for Thermally Activated Delayed Fluorescence: Impact of the Nature of Singlet vs Triplet Excited States. *J. Am. Chem. Soc.* **2017**, *139*, 4042–4051.
- (2) Uoyama, H.; Goushi, K.; Shizu, K.; Nomura, H.; Adachi, C. Highly Efficient Organic Light-Emitting Diodes from Delayed Fluorescence. *Nature* **2012**, *492*, 234–238.
- (3) Vázquez, R. J.; Kim, H.; Zimmerman, P. M.; Goodson, T. Using Ultra-Fast Spectroscopy to Probe the Excited State Dynamics of a Reported Highly Efficient Thermally Activated Delayed Fluorescence Chromophore. J. Mater. Chem. C 2019, 7, 4210–4221.
- (4) Gibson, J.; Penfold, T. J. Nonadiabatic Coupling Reduces the Activation Energy in Thermally Activated Delayed Fluorescence. *Phys. Chem. Chem. Phys.* **2017**, *19*, 8428–8434.
- (5) Gibson, J.; Monkman, A. P.; Penfold, T. J. The Importance of Vibronic Coupling for Efficient Reverse Intersystem Crossing in Thermally Activated Delayed Fluorescence Molecules. *ChemPhysChem* **2016**, 17, 2956–2961.
- (6) Hirata, S.; Sakai, Y.; Masui, K.; Tanaka, H.; Lee, S. Y.; Nomura, H.; Nakamura, N.; Yasumatsu, M.; Nakanotani, H.; Zhang, Q.; Shizu, K.; Miyazaki, H.; Adachi, C. Highly Efficient Blue Electroluminescence Based on Thermally Activated Delayed Fluorescence. *Nat. Mater.* **2015**, *14*, 330–336.
- (7) Liu, Y.; Li, C.; Ren, Z.; Yan, S.; Bryce, M. R. All-Organic Thermally Activated Delayed Fluorescence Materials for Organic Light-Emitting Diodes. *Nat. Rev. Mater.* **2018**, *3*, 18020.
- (8) Yang, Z.; Mao, Z.; Xie, Z.; Zhang, Y.; Liu, S.; Zhao, J.; Xu, J.; Chi, Z.; Aldred, M. P. Recent Advances in Organic Thermally Activated Delayed Fluorescence Materials. *Chem. Soc. Rev.* **2017**, *46*, 915–1016.
- (9) Kim, M.; Jeon, S. K.; Hwang, S.-H.; Lee, J. Y. Stable Blue Thermally Activated Delayed Fluorescent Organic Light-Emitting Diodes with Three Times Longer Lifetime than Phosphorescent Organic Light-Emitting Diodes. *Adv. Mater.* **2015**, *27*, 2515–2520.
- (10) Kim, M.; Jeon, S. K.; Hwang, S.-H.; Lee, S.-S.; Yu, E.; Lee, J. Y. Correlation of Molecular Structure with Photophysical Properties and Device Performances of Thermally Activated Delayed Fluorescent Emitters. *J. Phys. Chem. C* **2016**, *120*, 2485–2493.
- (11) Masui, K.; Nakanotani, H.; Adachi, C. Analysis of Exciton Annihilation in High-Efficiency Sky-Blue Organic Light-Emitting Diodes with Thermally Activated Delayed Fluorescence. *Org. Electron.* **2013**, *14*, 2721–2726.
- (12) Schinabeck, A.; Rau, N.; Klein, M.; Sundermeyer, J.; Yersin, H. Deep Blue Emitting Cu(i) Tripod Complexes. Design of High Quantum Yield Materials Showing TADF-Assisted Phosphorescence. *Dalton Trans.* **2018**, *47*, 17067–17076.
- (13) Rodriguez-Serrano, A.; Dinkelbach, F.; Marian, C. M. Intersystem Crossing Processes in The2CzPNemitter: A DFT/MRCI Study Including Vibrational Spin-Orbit Interactions. *Phys. Chem. Chem. Phys.* **2021**, 23, 3668–3678.
- (14) Vázquez, R. J.; Yun, J. H.; Muthike, A. K.; Howell, M.; Kim, H.; Madu, I. K.; Kim, T.; Zimmerman, P.; Lee, J. Y. New Direct Approach for Determining the Reverse Intersystem Crossing Rate in Organic Thermally Activated Delayed Fluorescent (TADF) Emitters. *J. Am. Chem. Soc.* **2020**, 142, 8074.
- (15) Adachi, C. Third-Generation Organic Electroluminescence Materials. *Jpn. J. Appl. Phys.* **2014**, *53*, 060101.
- (16) Yu, J. G.; Han, S. H.; Lee, H. L.; Hong, W. P.; Lee, J. Y. A Novel Molecular Design Employing a Backbone Freezing Linker for Improved Efficiency, Sharpened Emission and Long Lifetime in Thermally Activated Delayed Fluorescence Emitters. *J. Mater. Chem.* C 2019, 7, 2919–2926.
- (17) Chen, X. K.; Tsuchiya, Y.; Ishikawa, Y.; Zhong, C.; Adachi, C.; Brédas, J. L. A New Design Strategy for Efficient Thermally Activated

- Delayed Fluorescence Organic Emitters: From Twisted to Planar Structures. *Adv. Mater.* **2017**, *29*, 1–8.
- (18) Tsai, W.-L.; Huang, M.-H.; Lee, W.-K.; Hsu, Y.-J.; Pan, K.-C.; Huang, Y.-H.; Ting, H.-C.; Sarma, M.; Ho, Y.-Y.; Hu, H.-C.; Chen, C.-C.; Lee, M.-T.; Wong, K.-T.; Wu, C.-C. A Versatile Thermally Activated Delayed Fluorescence Emitter for Both Highly Efficient Doped and Non-Doped Organic Light Emitting Devices. *Chem. Commun.* 2015, *51*, 13662–13665.
- (19) Kim, I.; Cho, K. H.; Jeon, S. O.; Son, W.-J.; Kim, D.; Rhee, Y. M.; Jang, I.; Choi, H.; Kim, D. S. Three States Involving Vibronic Resonance Is a Key to Enhancing Reverse Intersystem Crossing Dynamics of an Organoboron-Based Ultrapure Blue Emitter. *J. Australas. Ceram. Soc.* 2021, 1, 987–997.
- (20) Choi, J.; Ahn, D.-S.; Oang, K. Y.; Cho, D. W.; Ihee, H. Charge Transfer-Induced Torsional Dynamics in the Excited State of 2,6-Bis(Diphenylamino)Anthraquinone. *J. Phys. Chem. C* **2017**, 121, 24317–24323.
- (21) He, G.; Zhou, L.-L.; Song, H.; Kuang, Z.; Wang, X.; Guo, Q.; Lu, H.-Y.; Xia, A. Insights into the Effect of Donor Ability on Photophysical Properties of Dihydroindeno[2,1-c] Fluorene-Based Imide Derivatives. *Phys. Chem. Chem. Phys.* **2018**, *20*, 7514–7522.
- (22) Franca, L. G.; Long, Y.; Li, C.; Danos, A.; Monkman, A. The Critical Role of $N\pi^*$ States in the Photophysics and Thermally Activated Delayed Fluorescence of Spiro Acridine-Anthracenone. *J. Phys. Chem. Lett.* **2021**, *12*, 1490–1500.
- (23) Lee, D. R.; Choi, J. M.; Lee, C. W.; Lee, J. Y. Ideal Molecular Design of Blue Thermally Activated Delayed Fluorescent Emitter for High Efficiency, Small Singlet-Triplet Energy Splitting, Low Efficiency Roll-off, and Long Lifetime. ACS Appl. Mater. Interfaces 2016, 8, 23190–23196.
- (24) Lee, D. R.; Hwang, S.-H.; Jeon, S. K.; Lee, C. W.; Lee, J. Y. Benzofurocarbazole and Benzothienocarbazole as Donors for Improved Quantum Efficiency in Blue Thermally Activated Delayed Fluorescent Devices. *Chem. Commun.* **2015**, *51*, 8105–8107.
- (25) Vázquez, R. J.; Kim, H.; Kobilka, B. M.; Hale, B. J.; Jeffries-El, M.; Zimmerman, P.; Goodson, T. Evaluating the Effect of Heteroatoms on the Photophysical Properties of Donor-Acceptor Conjugated Polymers Based on 2,6-Di(Thiophen-2-Yl)Benzo[1,2-b:4,5-B']Difuran: Two-Photon Cross-Section and Ultrafast Time-Resolved Spectroscopy. *J. Phys. Chem. C* 2017, 121, 14382—14392.
- (26) Williams, A. T. R.; Winfield, S. A.; Miller, J. N. Relative Fluorescence Quantum Yields Using a Computer-Controlled Luminescence Spectrometer. *Analyst* 1983, 108, 1067–1071.
- (27) Whitaker, J. E.; Haugland, R. P.; Moore, P. L.; Hewitt, P. C.; Reese, M.; Haugland, R. P. Cascade Blue Derivatives: Water Soluble, Reactive, Blue Emission Dyes Evaluated as Fluorescent Labels and Tracers. *Anal. Biochem.* **1991**, *198*, 119–130.
- (28) Reynolds, G. A. New Coumarin Dyes with Rigidized Structure for Flashlamp-Pumped Dye Lasers. *Opt Commun.* **1975**, *13*, 222.
- (29) Cai, Z.; Vázquez, R. J.; Zhao, D.; Li, L.; Lo, W.-y.; Zhang, N.; Wu, Q.; Keller, B.; Eshun, A.; Abeyasinghe, N.; Banaszak-Holl, H.; Goodson, T.; Yu, L. Two Photon Absorption Study of Low-Bandgap, Fully Conjugated Perylene Diimide-Thienoacene-Perylene Diimide Ladder-Type Molecules. *Chem. Mater.* **2017**, 29, 6726–6732.
- (30) Madu, I. K.; Muller, E. W.; Kim, H.; Shaw, J.; Burney-Allen, A. A.; Zimmerman, P.; Jeffries-El, M.; Goodson, T. Heteroatom and Side Chain Effects on the Optical and Photophysical Properties: Ultrafast and Nonlinear Spectroscopy of New Naphtho[1,2- b:5,6- B']Difuran Donor Polymers. J. Phys. Chem. C 2018, 122, 17049–17066.
- (31) Doan, P. H.; Pitter, D. R. G.; Kocher, A.; Wilson, J. N.; Goodson, T. Two-Photon Spectroscopy as a New Sensitive Method for Determining the DNA Binding Mode of Fluorescent Nuclear Dyes. J. Am. Chem. Soc. 2015, 137, 9198–9201.
- (32) Keller, B.; Cai, Z.; Muthike, A. K.; Sahu, P. K.; Kim, H.; Eshun, A.; Zimmerman, P. M.; Zhang, D.; Goodson, T. Investigating the Optical Properties of Thiophene Additions to S-Indacene Donors with Diketopyrrolopyrrole, Isoindigo, and Thienothiophene Acceptors. J. Phys. Chem. C 2018, 122, 27713–27733.

- (33) Taylor, E. L.; Metcalf, K. J.; Carlotti, B.; Lai, C.-T.; Modica, J. A.; Schatz, G. C.; Mrksich, M.; Goodson, T. Long-Range Energy Transfer in Protein Megamolecules. *J. Am. Chem. Soc.* **2018**, *140*, 15731–15743.
- (34) Abeywickrama, C. S.; Wijesinghe, K. J.; Plescia, C. B.; Fisher, L. S.; Goodson, T., III; Stahelin, R. V.; Pang, Y. A Pyrene-Based Two-Photon Excitable Fluorescent Probe to Visualize Nuclei in Live Cells. *Photochem. Photobiol. Sci.* **2020**, *19*, 1152–1159.
- (35) Devadas, M. S.; Kim, J.; Sinn, E.; Lee, D.; Goodson, T.; Ramakrishna, G. Unique Ultrafast Visible Luminescence in Monolayer-Protected Au 25 Clusters. *J. Phys. Chem. C* **2010**, *114*, 22417—22423.
- (36) Ashenfelter, B. A.; Desireddy, A.; Yau, S. H.; Goodson, T.; Bigioni, T. P. Fluorescence from Molecular Silver Nanoparticles. *J. Phys. Chem. C* **2015**, *119*, 20728–20734.
- (37) Varnavski, O.; Leanov, A.; Liu, L.; Takacs, J.; Goodson, T. Femtosecond Luminescence Dynamics in a Nonlinear Optical Organic Dendrimer. *Phys. Rev. B: Condens. Matter Mater. Phys.* **2000**, *61*, 12732–12738.
- (38) Donehue, J. E.; Varnavski, O. P.; Cemborski, R.; Iyoda, M.; Goodson, T. Probing Coherence in Synthetic Cyclic Light-Harvesting Pigments. *J. Am. Chem. Soc.* **2011**, *133*, 4819–4828.
- (39) Chai, J.-D.; Head-Gordon, M. Long-Range Corrected Hybrid Density Functionals with Damped Atom-Atom Dispersion Corrections. *Phys. Chem. Chem. Phys.* **2008**, *10*, 6615–6620.
- (40) Chai, J.-D.; Head-Gordon, M. Systematic Optimization of Long-Range Corrected Hybrid Density Functionals. *J. Chem. Phys.* **2008**, 128, 084106.
- (41) Beljonne, D.; Shuai, Z.; Pourtois, G.; Bredas, J. L. Spin-Orbit Coupling and Intersystem Crossing in Conjugated Polymers: A Configuration Interaction Description. *J. Phys. Chem. A* **2001**, *105*, 3899–3907.
- (42) Zhu, Q.; Guo, X.; Zhang, J. Theoretical Study on Photophysical Properties of a Series of Functional Pyrimidine-Based Organic Light-Emitting Diodes Emitters Presenting Thermally Activated Delayed Fluorescence. *J. Comput. Chem.* **2019**, *40*, 1578–1585.
- (43) Epifanovsky, É.; Gilbert, A. T. B.; Feng, X.; Lee, J.; Mao, Y.; Mardirossian, N.; Pokhilko, P.; White, A. F.; Coons, M. P.; Dempwolff, A. L.; Gan, Z.; Hait, D.; Horn, P. R.; Jacobson, L. D.; Kaliman, I.; Kussmann, J.; Lange, A. W.; Lao, K. U.; et al. Software for the Frontiers of Quantum Chemistry: An Overview of Developments in the Q-Chem 5 Package. *J. Chem. Phys.* **2021**, *155*, 084801.
- (44) Li, H.; Li, J.; Liu, D.; Huang, T.; Li, D. Effects of Electron Affinity and Steric Hindrance of the Trifluoromethyl Group on the π-Bridge in Designing Blue Thermally Activated Delayed Fluorescence Emitters. *Chem.*—*Eur. J.* **2020**, *26*, 6899–6909.
- (45) Suzuki, K.; Kubo, S.; Shizu, K.; Fukushima, T.; Wakamiya, A.; Murata, Y.; Adachi, C.; Kaji, H. Triarylboron-Based Fluorescent Organic Light-Emitting Diodes with External Quantum Efficiencies Exceeding 20. *Angew. Chem., Int. Ed.* **2015**, *54*, 15231–15235.
- (46) Wang, K.; Liu, W.; Zheng, C.-J.; Shi, Y.-Z.; Liang, K.; Zhang, M.; Ou, X.-M.; Zhang, X.-H. A Comparative Study of Carbazole-Based Thermally Activated Delayed Fluorescence Emitters with Different Steric Hindrance. *J. Mater. Chem. C* **2017**, *5*, 4797–4803.
- (47) Tanaka, H.; Shizu, K.; Nakanotani, H.; Adachi, C. Twisted Intramolecular Charge Transfer State for Long-Wavelength Thermally Activated Delayed Fluorescence. *Chem. Mater.* **2013**, *25*, 3766–3771.
- (48) Cho, Y.-J.; Lee, A.-R.; Kim, S.-Y.; Cho, M.; Han, W.-S.; Son, H.-J.; Cho, D. W.; Kang, S. O. The Influence of π -Conjugation on Competitive Pathways: Charge Transfer or Electron Transfer in New D- π -A and D- π -Si- π -A Dyads. *Phys. Chem. Chem. Phys.* **2016**, *18*, 22921–22928.
- (49) Hosokai, T.; Matsuzaki, H.; Nakanotani, H.; Tokumaru, K.; Tsutsui, T.; Furube, A.; Nasu, K.; Nomura, H.; Yahiro, M.; Adachi, C. Evidence and Mechanism of Efficient Thermally Activated Delayed Fluorescence Promoted by Delocalized Excited States. *Sci. Adv.* **2017**, 3, No. e1603282.
- (50) Yamaguchi, Y.; Matsubara, Y.; Ochi, T.; Wakamiya, T.; Yoshida, Z.-i. How the π Conjugation Length Affects the

- Fluorescence Emission Efficiency. J. Am. Chem. Soc. 2008, 130, 13867–13869.
- (51) Humbert-Droz, M.; Piguet, C.; Wesolowski, T. A. Fluorescence Quantum Yield Rationalized by the Magnitude of the Charge Transfer in π -Conjugated Terpyridine Derivatives. *Phys. Chem. Chem. Phys.* **2016**, *18*, 29387–29394.
- (52) Patterson, L. K.; Porter, G.; Topp, M. R. Oxygen Quenching of Singlet and Triplet States. *Chem. Phys. Lett.* **1970**, *7*, 612–614.
- (53) Lee, W.-H.; Lee, H.; Kim, J.-A.; Choi, J.-H.; Cho, M.; Jeon, S.-J.; Cho, B. R. Two-Photon Absorption and Nonlinear Optical Properties of Octupolar Molecules. *J. Am. Chem. Soc.* **2001**, *123*, 10658–10667.
- (54) Beerepoot, M. T. P.; Friese, D. H.; Ruud, K. Intermolecular Charge Transfer Enhances Two-Photon Absorption in Yellow Fluorescent Protein. *Phys. Chem. Chem. Phys.* **2014**, *16*, 5958–5964.
- (55) Sun, L.; Zhu, W.; Wang, W.; Yang, F.; Zhang, C.; Wang, S.; Zhang, X.; Li, R.; Dong, H.; Hu, W. Intermolecular Charge-Transfer Interactions Facilitate Two-Photon Absorption in Styrylpyridine—Tetracyanobenzene Cocrystals. *Angew. Chem., Int. Ed.* **2017**, *56*, 7831–7835.
- (56) Wang, X.; Wang, D.; Li, J.; Zhang, M.; Song, P. Physical Mechanism of Photoinduced Charge Transfer in Oneand Two-Photon Absorption in d-d-π-a Systems. *Materials* **2021**, *14*, 3925.
- (57) Zhang, W.; Kong, J.; Hu, D.; Tao, M.; Niu, X.; Vdović, S.; Aumiler, D.; Ma, Y.; Xia, A. Solvation-Dependent Excited-State Dynamics of Donor-Acceptor Molecules with Hybridized Local and Charge Transfer Character. J. Phys. Chem. C 2020, 124, 5574–5582.
- (58) Maffeis, V.; Brisse, R.; Labet, V.; Jousselme, B.; Gustavsson, T. Femtosecond Fluorescence Upconversion Study of a Naphthalimide-Bithiophene-Triphenylamine Push-Pull Dye in Solution. *J. Phys. Chem. A* **2018**, *122*, 5533–5544.
- (59) Ishimatsu, R.; Matsunami, S.; Shizu, K.; Adachi, C.; Nakano, K.; Imato, T. Solvent Effect on Thermally Activated Delayed Fluorescence by 1,2,3,5-Tetrakis(Carbazol-9-Yl)-4,6-Dicyanobenzene. *J. Phys. Chem. A* **2013**, *117*, 5607–5612.
- (60) Mataga, N.; Kaifu, Y.; Koizumi, M. Solvent Effects upon Fluorescence Spectra and the Dipolemoments of Excited Molecules. *Bull. Chem. Soc. Jpn.* **1956**, 29, 465–470.
- (61) Haseyama, S.; Niwa, A.; Kobayashi, T.; Nagase, T.; Goushi, K.; Adachi, C.; Naito, H. Control of the Singlet—Triplet Energy Gap in a Thermally Activated Delayed Fluorescence Emitter by Using a Polar Host Matrix. *Nanoscale Res. Lett.* **2017**, *12*, 268.
- (62) Cotts, B. L.; McCarthy, D. G.; Noriega, R.; Penwell, S. B.; Delor, M.; Devore, D. D.; Mukhopadhyay, S.; De Vries, T. S.; Ginsberg, N. S. Tuning Thermally Activated Delayed Fluorescence Emitter Photophysics through Solvation in the Solid State. *ACS Energy Lett.* **2017**, *2*, 1526–1533.
- (63) Abdel-Shafi, A. A.; Worrall, D. R. Mechanism of the Excited Singlet and Triplet States Quenching by Molecular Oxygen in Acetonitrile. *J. Photochem. Photobiol., A* **2005**, *172*, 170–179.
- (64) McGown, L. B.; Nithipatikom, K. Molecular Fluorescence and Phosphorescence. *Appl. Spectrosc. Rev.* **2000**, *35*, 353–393.
- (65) Goushi, K.; Yoshida, K.; Sato, K.; Adachi, C. Organic Light-Emitting Diodes Employing Efficient Reverse Intersystem Crossing for Triplet-to-Singlet State Conversion. *Nat. Photonics* **2012**, *6*, 253–258.
- (66) Lee, H. L.; Lee, K. H.; Lee, J. Y. Indoloindole as a New Building Block of a Hole Transport Type Host for Stable Operation in Phosphorescent Organic Light-Emitting Diodes. *J. Mater. Chem.* C **2019**, *7*, 5988–5994.
- (67) Jung, M.; Lee, K. H.; Lee, J. Y. Molecular Engineering of Isomeric Benzofurocarbazole Donors for Photophysical Management of Thermally Activated Delayed Fluorescence Emitters. *Chem.—Eur. J.* **2020**, *26*, 4816–4821.
- (68) Byeon, S. Y.; Kim, J.; Lee, D. R.; Han, S. H.; Forrest, S. R.; Lee, J. Y. Nearly 100% Horizontal Dipole Orientation and Upconversion Efficiency in Blue Thermally Activated Delayed Fluorescent Emitters. *Adv. Opt. Mater.* **2018**, *6*, 1701340.

(69) Sun, J. W.; Kim, K.-H.; Moon, C.-K.; Lee, J.-H.; Kim, J.-J. Highly Efficient Sky-Blue Fluorescent Organic Light Emitting Diode Based on Mixed Cohost System for Thermally Activated Delayed Fluorescence Emitter (2CzPN). ACS Appl. Mater. Interfaces 2016, 8, 9806–9810.

(70) Kang, J. S.; Hong, T. R.; Kim, H. J.; Son, Y. H.; Lampande, R.; Kang, B. Y.; Lee, C.; Bin, J.-K.; Lee, B. S.; Yang, J. H.; Kim, J.; Park, S.; Cho, M. J.; Kwon, J. H.; Choi, D. H. High-Performance Bipolar Host Materials for Blue TADF Devices with Excellent External Quantum Efficiencies. *J. Mater. Chem. C* **2016**, *4*, 4512–4520.

□ Recommended by ACS

Photophysical Properties of Thermally Activated Delayed Fluorescent Materials upon Distortion of Central Axis of Donor Moiety

Hyung Suk Kim, Min Chul Suh, et al.

NOVEMBER 21, 2018

THE JOURNAL OF PHYSICAL CHEMISTRY C

READ 🗹

Excited-State Modulation in Donor-Substituted Multiresonant Thermally Activated Delayed Fluorescence Emitters

Sen Wu, Eli Zysman-Colman, et al.

MAY 09, 2022

ACS APPLIED MATERIALS & INTERFACES

READ **C**

Kinetics of Triplet Exciton Energy-Transfer Processes in Triplet Sensitizer-Doped Fluorescent Polymers

Amrita Dey and Dinesh Kabra

MAY 22, 2019

THE JOURNAL OF PHYSICAL CHEMISTRY A

READ 🗹

Investigation of Thermally Activated Delayed Fluorescence from a Donor-Acceptor Compound with Time-Resolved Fluorescence and Density Functional...

Reinhard Scholz, Sebastian Reineke, et al.

FEBRUARY 05, 2020

THE JOURNAL OF PHYSICAL CHEMISTRY A

READ 🗹

Get More Suggestions >